Materials Science & Engineering A 821 (2021) 141639

Contents lists available at ScienceDirect

Materials Science & Engineering A

journal homepage: www.elsevier.com/locate/msea

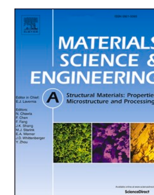

Excellent mechanical properties and high electrical conductivity of Cu-Co-Si-Ti alloy due to multiple strengthening

Yongfeng Geng [a,1], Yijie Ban [a,1], Xu Li [d], Yi Zhang [a,b,c,*], Yanlin Jia [e,**], Baohong Tian [a,b,c], Meng Zhou [a,b,c,***], Yong Liu [a,b,c], Alex A. Volinsky [f,g], Kexing Song [a,b,c,****], Shunlong Tang [a]

[a] School of Materials Science and Engineering, Henan University of Science and Technology, Luoyang, 471023, PR China
[b] Provincial and Ministerial Co-construction of Collaborative Innovation Center for Non-ferrous Metal New Materials and Advanced Processing Technology, Henan Province, Luoyang, 471023, PR China
[c] Henan Province Key Laboratory of Nonferrous Materials Science and Processing Technology, Luoyang, 471023, PR China
[d] Center for Advanced Measurement Science, National Institute of Metrology, Beijing, 100029, PR China
[e] College of Materials Science and Engineering, Central South University, Changsha, 410083, China
[f] Department of Mechanical Engineering, University of South Florida, Tampa, 33620, USA
[g] National Research Tomsk State University, 36 Lenin Ave., Tomsk, 634050, Russia

A R T I C L E I N F O

Keywords:
Cu-Co-Si and Cu-Co-Si-Ti alloys
Precipitation
Multiple strengthening
Mechanical properties

A B S T R A C T

The high performance of copper alloys is widely welcomed due to their high electrical conductivity and excellent mechanical properties. These alloys are mainly used in electrical, electronic and aerospace fields. In the present work, we proposed a new class of Cu-Co-Si-Ti alloys by incorporating the multiple alloying elements, resulting in the multiple strengthening during heat treatment. It can be observed that Ti addition can significantly improve the micro-hardness of the Cu-Co-Si-alloy. Solution strengthening, deformation strengthening and dual-nanoprecipitation strengthening led to the Cu-Co-Si-Ti alloy with excellent tensile strength (617.9 MPa) and high electrical conductivity (41.7% IACS) using the optimal process of cold rolling by 50% and aging at 500 °C for 30 min. Electron backscatter diffraction technology was used to analyze the microstructure and texture evolution during the copper alloys aging process. It was found that the volume fraction of Goss, Brass, copper and S texture had close connections with the mechanical properties. From multiple strengthening mechanisms, the dual nanoprecipitation strengthening contributed the most due to the nanoprecipitation of Co_2Si and Cu_4Ti.

1. Introduction

Copper alloys are widely used in electrical, electronic, aerospace and other fields due to their high electrical and thermal conductivity, excellent mechanical properties, stable performance and long service life [1–6]. The high strength of copper alloys is mainly attributed to the precipitation of nano-precipitates during aging [7]. With the development of all kinds of components in the direction of more precision, higher requirements are put forward for the performance of copper alloys, which are closely related to the improvement of people's living standards. Cu-Ni-Si alloy is a typical aging strengthening alloy with the characteristics of high elasticity, strength and conductivity, which is expected to replace high elastic beryllium bronze [8–10]. Therefore, further researches are required to improve the strength of Cu-Ni-Si alloys by understanding and optimizing the aging process.

A large number of basic researches on Cu-Ni-Si-X alloys have been carried out for a long time in the past few years. Wu et al. [11] demonstrated that the deformation-induced defects improved the precipitation and the number density of precipitates, resulting in the improvement of both conductivity and mechanical properties. Yi et al. [7] found a new orientation relationship between the precipitates and the Cu matrix in the over-aged condition and put forward a coarsening

* Corresponding author. School of Materials Science and Engineering, Henan University of Science and Technology, Luoyang, 471023, PR China.
** Corresponding author.
*** Corresponding author. School of Materials Science and Engineering, Henan University of Science and Technology, Luoyang, 471023, PR China.
**** Corresponding author. School of Materials Science and Engineering, Henan University of Science and Technology, Luoyang, 471023, PR China.
E-mail addresses: yizhang@haust.edu.cn, zhshgu436@163.com (Y. Zhang), jiayanlin@126.com (Y. Jia), zhoumeng0902@126.com (M. Zhou), kxsong123@163.com (K. Song).
[1] These authors contributed equally to this work.

https://doi.org/10.1016/j.msea.2021.141639
Received 3 March 2021; Received in revised form 20 June 2021; Accepted 22 June 2021
Available online 24 June 2021
0921-5093/© 2021 Elsevier B.V. All rights reserved.

mechanism of the metastable precipitates. Kim et al. [12] observed the nano-twins in cold-drawn Cu-Ni-Si alloys, which show little effect on the conductivity of copper alloys while effectively interfering with the dislocation movement, and they are one of the key factors endowing copper alloys with the trade-off characteristics of high strength and conductivity. Multi-precipitation phases of Ni_2Si, γ′-Ni_3Al, β-Ni_3Si showed a significant influence on the strengthening effects during the aging process of Cu-Ni-Si alloy [13], and the low electron diffraction influence of Mg and Cr contributed to both solution strengthening and maintaining a high electrical conductivity. Wang et al. [14] confirmed the presence of δ-Ni_2Si precipitates by TEM, which strengthened the Cu-Ni-Si alloy through the Orowan mechanism. In addition, there are also many studies on Cu-Ni-Co-Si alloys due to the similar properties of Co and Ni [15–18]. However, there are few investigations on the analysis of microstructure evolution and the relationship between texture and mechanical properties of the copper alloys during the aging process by the electron backscatter diffraction (EBSD) technology, which need to be further investigated.

In our previous work, based on a large number of researches on Cu-Ni-Si and Cu-Ni-Co-Si alloys, we proposed to replace Ni completely with Co and obtained a new class of Cu-Co-Si-(Ti) alloys. The hot deformation was carried out on the Gleeble-1500 simulator to understand the hot deformation studies. In addition, Ti and Ce addition on the flow stress and microstructure evolution were investigated by EBSD and TEM [19, 20]. In the present work, the precipitation behavior of Cu-Co-Si-(Ti) alloys was investigated by scanning electron microscope (SEM), EBSD, transmission electron microscope (TEM) and high-resolution transmission electron microscope (HRTEM). Moreover, the nanoscale strain field generated by nanoscale twins was analyzed by the geometric phase analysis (GPA). The optimum aging parameters with comprehensive properties were obtained by the combination of solid solution strengthening, deformation strengthening, grain boundaries strengthening and aging strengthening. In addition, the effects of Ti addition on the electrical conductivity, micro-hardness and texture evolution were analyzed.

2. Materials and methods

The specific smelting methods of the Cu-1.0Co-0.65Si and Cu-1.0Co-0.65Si-0.1Ti alloys have been introduced in detail in our previous work [19,20], so we will not introduce it too much here. The molten ingots were homogenized annealed at 980 °C for 1 h in a vacuum heat treatment furnace, and then hot-rolled in order to eliminate casting defects and densify the microstructure. The hot-rolled samples were treated with solution treatment at 960 °C for 1 h to make solute atoms melt into the matrix, followed by cutting into 1 × 10 × 100 mm sheets. The sheets were further cold rolled up to 50% thickness reduction (0.5 mm). To investigate the influence of additional heat treatment on the precipitation behavior of Cu-Co-Si and Cu-Co-Si-Ti alloys and obtain the high comprehensive properties, the cold-rolled sheets were aged in the range between 400 °C and 550 °C for a different time in a vacuum furnace, followed by air cooling. The corresponding schematic diagram of the experiment was shown in Fig. 1. Ultimately, the samples before and after aging were tested for electrical conductivity (ZY9987 digital micro-ohm meter) and micro-hardness (HVS-1000 hardness tester), and the tensile strength of the samples with the highest hardness was tested by the AG-I 250 KN machine with a speed of 5.0 mm/min at room temperature. It should be pointed out that all the above measurements were carried out at room temperature. Before the hardness test measurement, each sample should be polished to ensure that the indentation contour was clear and the field of vision was clear, to improve the accuracy of the measured value. Each sample was measured five times to get the average value with the load of 100 g and the loading time of 10 s.

The microstructure evolution during the aging process was observed by SEM, EBSD, TEM and HRTEM. For SEM observation carried out on the JSM-7800F backscatter scanning electron microscope, the samples were rough ground on different types of sandpaper, and then polished on the polishing machine. In addition, the EBSD tests in different states were also carried out on the JSM-7800F backscatter scanning electron microscope, which was mechanically polished to remove the rough scratches, followed by the electro-polishing for 1 min with DC power supply and magnetic stirrer in a solution of 50% CH_3CH_2OH and 50% H_3PO_4 at a voltage of 5 V at 25 °C. The TEM sample, carried out on FEI Talos F200X and JEM-2100 transmission electron microscope, was prepared by mechanical polishing to a thickness of about 50 μm and then thinned by Gatan 695 ion thinner. The sample thinning parameters were ion beam energy 5kev, ion gun angle ±8° thinning to hole, 4.5kev ± 6° thinning for 5min, 4kev ± 4° thinning for 5min, 3kev ± 3° thinning for 5min.

3. Results

3.1. Conductivity and mechanical properties

In the aging process, it is very important to investigate the crystallographic characteristics of the Cu-Co-Si-Ti alloy in different states for analyzing its strengthening and conducting mechanism. After solution treatment, the Co, Si and Ti elements were dissolved into the copper matrix to form a supersaturated solid solution, which can be observed in Fig. 2 with the element content of 0.45%, 0.28% and 0% for solute atoms

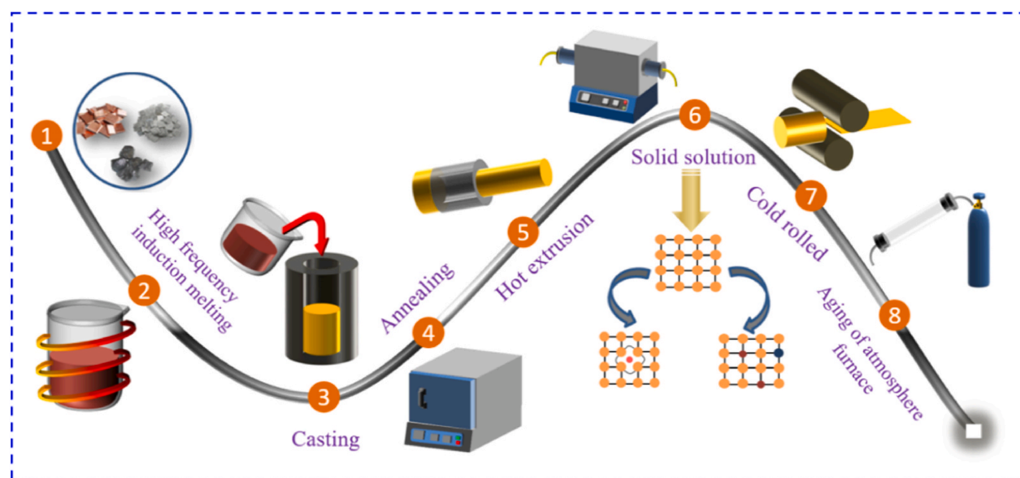

Fig. 1. Schematic diagram of the experiment for Cu-Co-Si and Cu-Co-Si-Ti alloys.

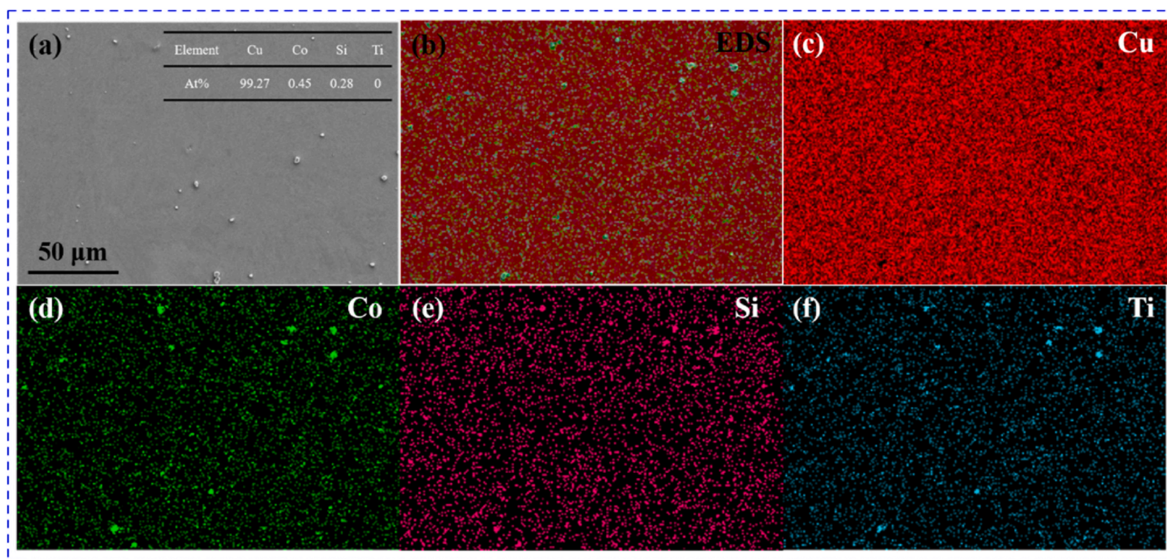

Fig. 2. Element distribution after solution treatment of Cu-Co-Si-Ti alloy: (a) electronic image, (b) EDS map, (c) surface scan distribution of Cu, (d) surface scan distribution of Co, (e) surface scan distribution of Si, (f) surface scan distribution of Ti.

(Co, Si and Ti). And then the supersaturated solid solution spontaneously decomposed in the aging process, forming new phases in the form of precipitates, which improved the strength of the Cu-Co-Si-Ti alloy and had high conductivity, simultaneously. Compared with the element distribution in Fig. 2, a significant increase in the content of solute atoms (1.05%, 0.59% and 0.1%) can be observed from Fig. 3. Moreover, it can be seen that the element distributions were more uniform after the aging process.

In order to determine the effects of Ti addition on the aging behavior of Cu-Co-Si alloy and obtain the optimum aging parameters that result in the superior performance of the Cu-Co-Si-Ti alloy, the variations in micro-hardness and electrical conductivity of Cu-Co-Si and Cu-Co-Si-Ti alloys at different aging temperatures for various times were investigated. Fig. 4 shows the electrical conductivity and mechanical properties of Cu-Co-Si and Cu-Co-Si-Ti alloys under different aging temperatures (400 °C–550 °C) for various times. It can be seen that there were three main stage during the aging process, including under-aging stage, peak-aging stage and over-aging stage [11,13,17]. In the under-aging stage, the micro-hardness increased rapidly, which can be attributed to that the super saturation of the copper alloy was strong at the early stage of aging, and the precipitation force and precipitation rate of the second phase were large at this time. The micro-hardness reached the maximum, corresponding to the peak-aging stage, due to the precipitation rate reaching the maximum at this stage. With the further prolongation of aging time, the micro-hardness began to decrease, corresponding to the over-aging stage, which can be attributed to the grown-up precipitates and softening effect caused by the release of lattice distortion energy [21,22]. In addition, precipitation is a diffusion process of atoms. With the increasing of aging temperature, the activity of atoms is stronger, promoting the precipitation, namely, the higher of aging temperature, the higher micro-hardness of the Cu-Co-Si-Ti alloy. With the temperature exceeding a certain limit, the micro-hardness decreases with the increasing of temperature, which can be attributed to the over-aging stage to the growth of the precipitates and softening effect caused by the release of lattice distortion energy. As illustrated in Fig. 4(a) and (b), the micro-hardness of the Cu-Co-Si and Cu-Co-Si-Ti

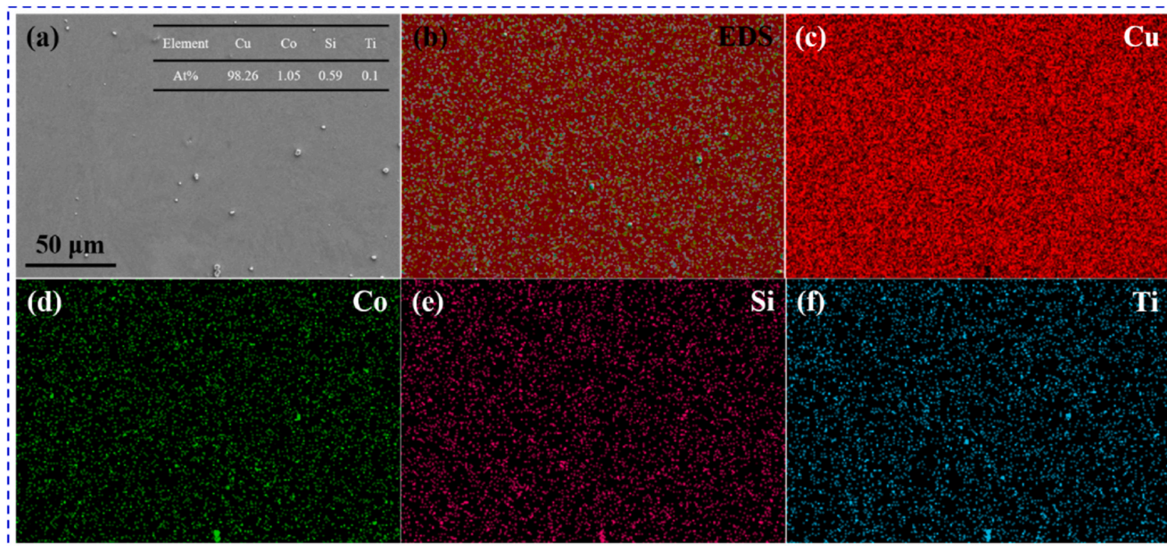

Fig. 3. Element distribution of Cu-Co-Si-Ti alloy after aging process: (a) electronic image, (b) EDS map, (c) surface scan distribution of Cu, (d) surface scan distribution of Co, (e) surface scan distribution of Si, (f) surface scan distribution of Ti.

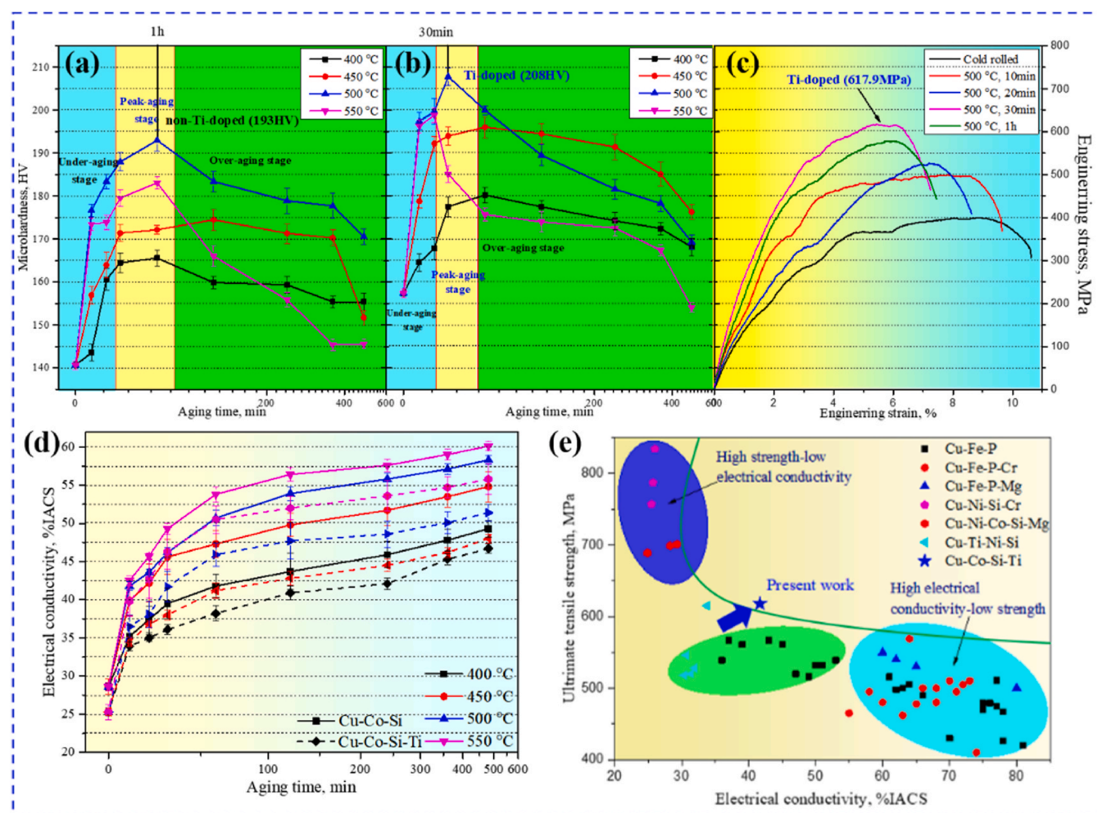

Fig. 4. Mechanical properties and electrical conductivity of Cu-Co-Si and Cu-Co-Si-Ti alloys aging at different temperatures: (a) micro-hardness of Cu-Co-Si alloy, (b) micro-hardness of Cu-Co-Si-Ti alloy, (c) tensile strength of Cu-Co-Si-Ti alloy under different conditions, (d) electrical conductivity of the two alloys aging at different temperatures, (e) comparison of tensile strength vs. electrical conductivity between the present Cu-Co-Si-Ti alloy and conventional copper alloys [9,11,13,17,23–30].

alloys increased rapidly in the under-aging stage, reaching the peak aging stage in a short time, and then decreased with a further increase in the aging time at all selected temperatures. For example, the micro-hardness of Cu-Co-Si alloy aging at 500 °C from 10 min to 480 min were 176 HV, 183 HV, 188 HV, 193 HV, 183 HV, 179 HV, 177 HV and 171 HV, respectively. The peak values of Cu-Co-Si alloy aging at 400 °C–550 °C were 165 HV for 60 min, 174 HV for 120 min, 193 HV for 60 min and 183 HV for 60 min, respectively. Moreover, the corresponding peak values of Cu-Co-Si-Ti alloy were 180 HV for 60 min, 196 HV for 60 min, 208HV for 30 min and 199 HV for 20 min, respectively. We take Cu-Co-Si-Ti alloy as an example to carry out tensile test aging at 500 °C for different times, and the tensile curves are shown in Fig. 4(c). It can be obtained that the tensile strength under different conditions were 499.6 MPa, 526.8 MPa, 617.9 MPa and 578.7 MPa, respectively, higher than that of under cold rolled conditions. Instead, the plasticity of the Cu-Co-Si-Ti alloy was opposite to the strength.

Besides, the electrical conductivity of the Cu-Co-Si and Cu-Co-Si-Ti alloys also increased dramatically in the under-aging stage, which can be attributed to the precipitation of precipitates and the reduction of electron scattering, as shown in Fig. 4(d). Finally, electrical conductivity curves showed a slow-growth trend. For example, the electrical conductivity of Cu-Co-Si alloy aging at 500 °C from 10 min to 480 min were 41.8 %IACS, 43.6 %IACS, 46.2 %IACS, 50.7 %IACS, 53.9 %IACS, 55.8 % IACS, 57.1 %IACS and 58.3 %IACS, respectively. The number and size of solute atoms dissolved in the matrix are the main factors affecting the electrical conductivity of the copper alloy [9,11]. The grain boundaries and elements dissolved in the alloy will distort the matrix, increase the scattering of electrons and reduce the electrical conductivity of the alloy. With the increasing of aging temperature, the alloy elements precipitated rapidly from the supersaturated matrix in the form of precipitates, softening effect was strengthened caused by the release of lattice distortion energy in the aging process, and the electron scattering was reduced, resulting in the increasing of electrical conductivity for the Cu-Co-Si and Cu-Co-Si-Ti alloys. For example, the electrical conductivity of Cu-Co-Si alloy aging at 60 min from 400 °C to 550 °C were 41.8 % IACS, 47.3 %IACS, 50.7 %IACS and 53.8 %IACS and 58.3 %IACS, respectively.

By connecting the electrical conductivity and micro-hardness of the Cu-Co-Si and Cu-Co-Si-Ti alloys, the peak aging properties can be determined to be 193 HV, 50.7 %IACS aging at 500 °C for 60 min and 208HV, 41.7%IACS aging at 500 °C for 30 min, respectively with increasing by 7.8% for micro-hardness. It can be seen that Ti addition significantly increased the micro-hardness based on sacrificing part of the electrical conductivity of the Cu-Co-Si-Ti alloy according to Fig. 4(a and b) and 4(d). Moreover, it can be also observed that Ti addition shortened the aging time to reach the peak aging stage for the Cu-Co-Si-Ti alloy (60 min for Cu-Co-Si alloy and 30 min for Cu-Co-Si-Ti alloy).

The tensile strength can be measured by tensile tests of samples under different states (Fig. 4(a and b)), and the highest tensile strength is 617.9 MPa for Cu-Co-Si-Ti alloy aging at 500 °C for 30 min. Ultimately, the optimum aging parameters of Cu-Co-Si-Ti alloy were aging at 500 °C for 30 min with the properties of 208 HV, 617.9 MPa and 41.7% IACS. The comparison of tensile strength and electrical conductivity between the present Cu-Co-Si-Ti alloy and conventional copper alloys was shown in Fig. 4(e), where can be seen that the present work for Cu-Co-Si-Ti alloy has a good comprehensive property.

Dimple is the main microscopic feature of metal plastic fracture. It is the mark left on the surface of the fracture after the micro cavity produced by the plastic deformation of the material in the micro area, which leads to the fracture through nucleation, growth, aggregation and finally connected with each other. The size of dimple includes average diameter and depth [31,32]. Generally, under the same fracture conditions, the larger the dimple size, the better the plasticity of the material. Fig. 5 shows the SEM micrographs showing fracture surface aging at

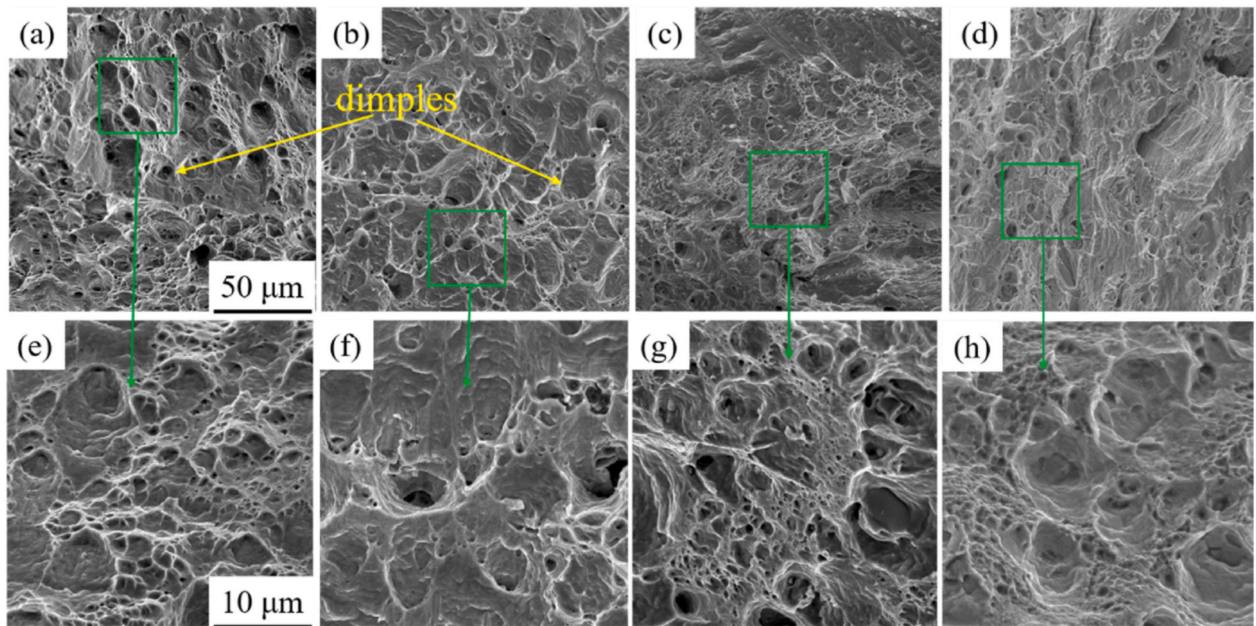

Fig. 5. SEM micrographs showing fracture surface aging at 500 °C for different time: (a) (e) 10 min, (b) (f) 20 min, (c) (g) 30 min, (d) (h) 60 min.

500 °C for a different time. For the condition of aging at 500 °C for 10 min (Fig. 5(a) and (e)), there were a lot of equiaxial dimples on the fracture surface, implying the shear fracture mode. Serpentine sliding and the sharp tearing edges can be observed on the dimple walls, i.e., the fracture mechanism is micro-voids coalescence. With the aging time reaching the peak stage (30 min), the number and size of dimples decreased significantly, as illustrated in Fig. 5(c) and (g), which were consistent with the high strength and poor ductility.

3.2. EBSD analysis

To investigate the effects of Ti addition on microstructure evolution and micro texture of Cu-Co-Si and Cu-Co-Si-Ti alloys during aging treatment, electron backscattering diffraction (EBSD) technology was

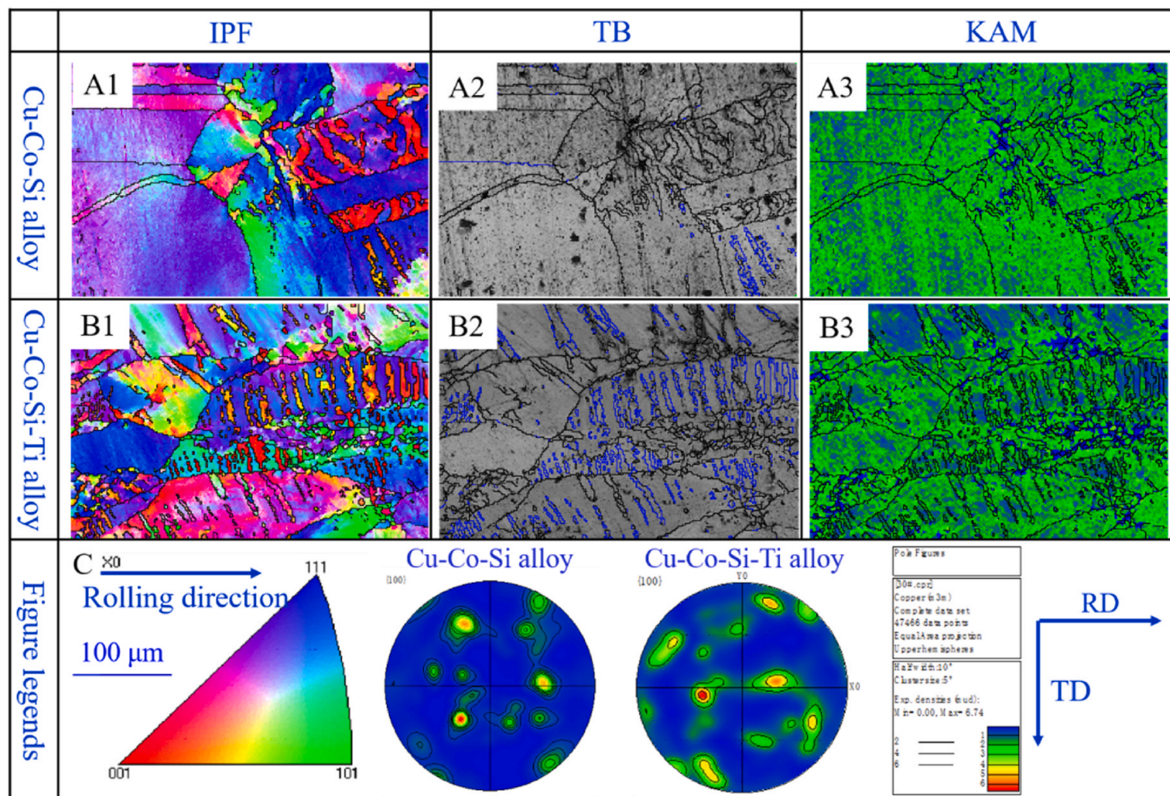

Fig. 6. EBSD-IPF, TB and corresponding KAM maps of Cu-Co-Si alloy aging at 500 °C for 60 min (A1-A3), EBSD-IPF, TB and corresponding KAM maps of Cu-Co-Si-Ti alloy aging at 500 °C for 30 min (B1-B3), Corresponding figure legends and pole figures (C).

used to observe the microstructure and texture evolution under different aging conditions. Fig. 6 shows the EBSD-inverse pole figure (IPF) maps, twin boundaries (TB) maps, Kernel Average Misorientation (KAM) maps and corresponding figure legends of Cu-Co-Si and Cu-Co-Si-Ti alloys aging at 500 °C for 60 min and 30 min, respectively. As illustrated in Fig. 6(A1-A3), several twins were observed in Cu-Co-Si alloy after aging at 500 °C for 60 min, indexed by blue grain boundaries. However, more twins appeared in the Cu-Co-Si-Ti alloy due to the addition of Ti, as given in Fig. 6(B1-B3). The corresponding micro-texture also changed significantly, which can be obtained from Fig. 6(C). In order to analyze the micro-texture evolution with non-Ti doped and Ti-doped, the pole figures and 3D-ODF maps of Cu-Co-Si and Cu-Co-Si-Ti alloys aging at 500 °C for a different time were obtained (Fig. 7), respectively. It can be observed that the maximum texture intensity for Cu-Co-Si alloy was 6.09 mud (Fig. 7(h)). Surprisingly, the maximum texture intensity increased to 6.74 mud for Cu-Co-Si-Ti alloy due to the Ti addition, as given in Fig. 7(i). Taking Cu-Co-Si-Ti alloy as an example, we illustrated the ideal texture component maps of Cube texture, Goss texture, Brass texture, copper texture, S texture, <111>//X, <110>//X and <100>//X in Fig. 7(a–g). The volume fraction of ideal texture components of Cu-Co-Si and Cu-Co-Si-Ti alloys can be observed in Fig. 7(j). In addition, the volume fraction for the ideal texture components of {001} <100> Cube texture, {011} <100> Goss texture, {011} <112> Brass texture, {112} <111> copper texture, S texture, <111>//X, <110>//X and <100>//X in Cu-Co-Si alloy were 5.6%, 4.96%, 14.3%, 15.3%, 9.6%, 18.9%, 30.3% and 29%, respectively. Corresponding volume fraction for the ideal texture components of Cu-Co-Si-Ti alloy were 3.17%, 7.01%, 16.4%, 25%, 14.7%, 12.8%, 24.4% and 38.5%, respectively. It can be observed that the volume fraction of the main deformation texture components, including Goss texture, Brass texture, copper texture and S texture, increased due to the Ti addition, indicating a slight texture strengthening.

Fig. 8 shows the EBSD-IPF map, TB map, corresponding KAM map and figure legends of Cu-Co-Si-Ti alloy aging at 500 °C for 120 min. It can be seen that there were still some twins in the microstructure due to deformation. After aging for 30 min (Fig. 6(B1-B3)), a small amount of recrystallization had occurred, that is, a small amount of recrystallized grains appeared in the interior. With the increasing of aging time, the grains had grown up obviously (Fig. 8(a)). Compared with Fig. 6(B1-B3) and Fig. 8(a–c), the number of twins and internal strain decreased correspondingly due to the increase of aging time. In addition, after aging for a different time, the crystal orientation of the Cu-Co-Si-Ti alloy changed obviously according to the pole figures, which can be seen from Figs. 6(C) and Fig. 8(d).

Fig. 9(a) shows the pole figures and 3D-ODF map of Cu-Co-Si-Ti alloy aging at 500 °C for 120 min. It can be observed that the maximum texture intensity for Cu-Co-Si-Ti alloy was 6.65 mud, slightly lower than that in 30 min. In addition, the volume fraction of ideal texture components for Cu-Co-Si-Ti alloy aging at 500 °C for 30 min and 120 min can be observed in Fig. 9(b). The volume fraction for the ideal texture components of Cube texture, Goss texture, Brass texture, copper texture, S texture, <111>//X, <110>//X and <100>//X in Cu-Co-Si alloy were 7.35%, 1.43%, 12.4%, 2.7%, 4.67%, 25.6%, 41.3% and 22%, respectively. Taking the fiber texture as an example, the main fiber orientation after aging for 30 min was <111>//X, while the main fiber orientation after aging for 120 min were <110>//X and <100>//X. With the prolonged of aging time, the volume fraction of main texture components decreased, whereas the fraction of randomly oriented grains increased, indicating a slight texture weakened [33]. In other words, the random texture was developed in the samples aging for 120 min by the

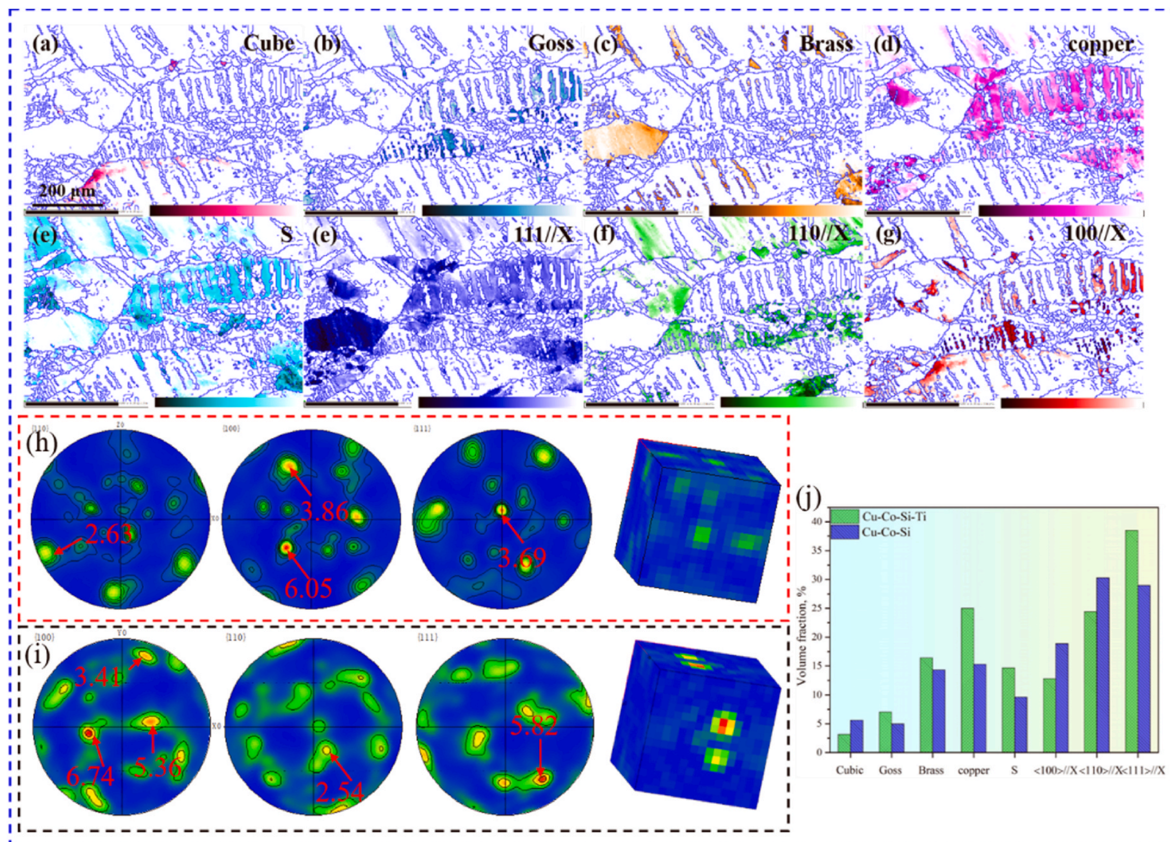

Fig. 7. Texture composition of Cu-Co-Si-Ti alloy aging at 500 °C for 30 min: (a) Cube texture, (b) Goss texture, (c) Brass texture, (d) copper texture, (e) S texture, (f) <111>//X, (g) <110>//X, (h) <100>//X, (h) pole figures and 3D-ODF map of Cu-Co-Si alloy aging at 500 °C for 60 min, (i) pole figures and 3D-ODF map of Cu-Co-Si-Ti alloy aging at 500 °C for 30 min, (j) texture composition of Cu-Co-Si and Cu-Co-Si-Ti alloys aging at 500 °C for 60 min and 30 min.

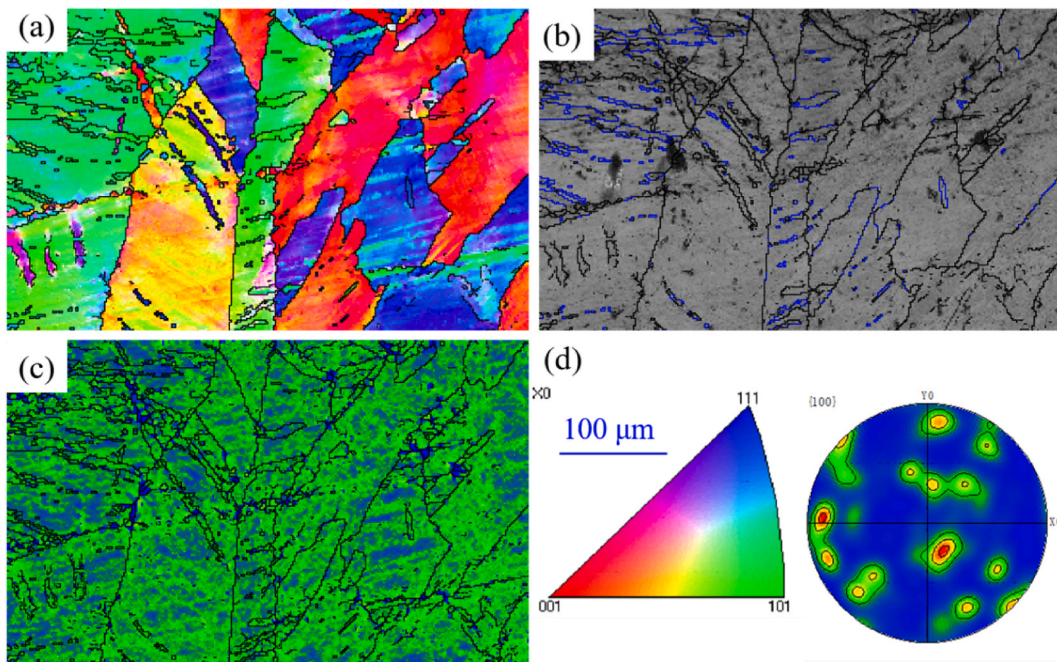

Fig. 8. EBSD-IPF, TB and corresponding KAM maps of Cu-Co-Si-Ti alloy aging at 500 °C for 120 min: (a) IPF map, (b) TB map, (c) KAM map, (d) Corresponding figure legends and pole figures.

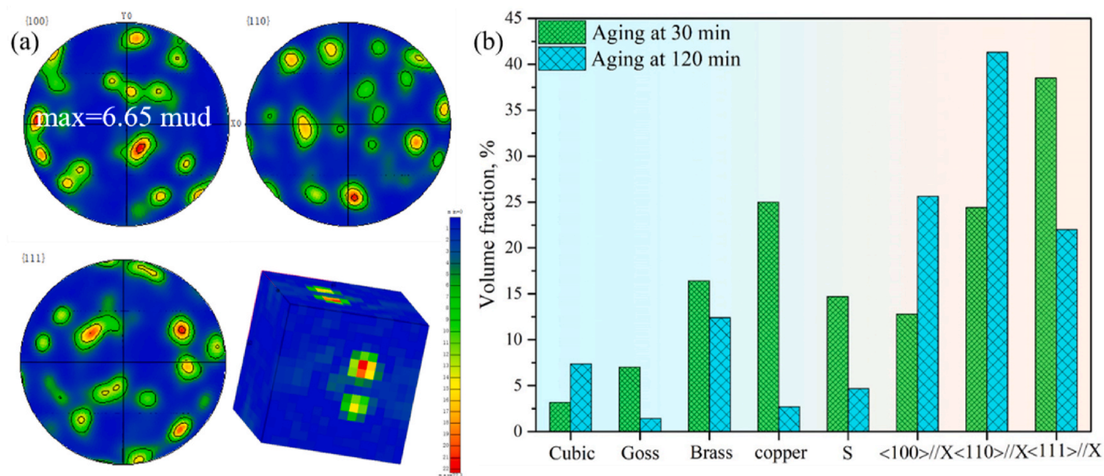

Fig. 9. (a) Pole figures and 3D-ODF map of Cu-Co-Si-Ti alloy aging at 500 °C for 120 min, (b) texture composition of Cu-Co-Si-Ti alloy aging at 500 °C for 30 min and 120 min.

progression of recrystallization, resulting in a weaker texture.

3.3. TEM analysis

In this section, we took the Cu-Co-Si-Ti alloy as an example to analyze the microstructure characterization during the aging process. Fig. 10 shows the TEM and HRTEM micrographs of Cu-Co-Si-Ti alloy aging at 500 °C for 30 min. It can be observed that there was a typical deformation structure in the microstructure, including deformation bands, dislocation entanglement, twins and et al., which can be observed from Fig. 10(a–c). It should be noted that the dislocation density inside the twins was higher, while that around the twin boundaries was lower, which may be attributed to the decreasing of dislocation density due to the consumption of surrounding dislocations by the formation of twins [34,35]. The above results can be observed from the GPA analysis in Fig. 10(e). There were obvious edge dislocations in the matrix due to the cold deformation, as given by the HRTEM image taken from $<111>_{Cu}$ in Fig. 10(i). The supersaturated solid solution will decompose spontaneously and precipitate a new nano-phase during aging [17,24]. After aging at 500 °C for 30 min, two kinds of precipitates (Fig. 10(f) and (g)) precipitated from the copper matrix, which can be determined to be Co_2Si from Fig. 11(a–c) and Cu_4Ti from Fig. 11(d and e), respectively. Fig. 11(a) shows the three plane directions of $(2\overline{2}0)_{Co2Si}$, $(30\overline{1})_{Co2Si}$ and $(12\overline{1})_{Co2Si}$ for Co_2Si with orthorhombic structure, as exemplified in Fig. 11(h). Moreover, Fig. 11(d) shows the three plane directions of $(013)_{Cu4Ti}$, $(112)_{Cu4Ti}$ and $(10\overline{1})_{Cu4Ti}$ for Cu_4Ti with orthorhombic structure (Fig. 11(i)). According to the periodic contrast difference of the high-resolution atomic images shown in Fig. 11(f) and (g), a tri-layered periodicity exists in a selected Cu_4Ti-phase nanodomain with the crystal plane spacing of 0.425 nm for $(10\overline{1})_{Cu4Ti}$. Ti atoms were enriched in this orientation with three atomic layers per cycle, indicating that the

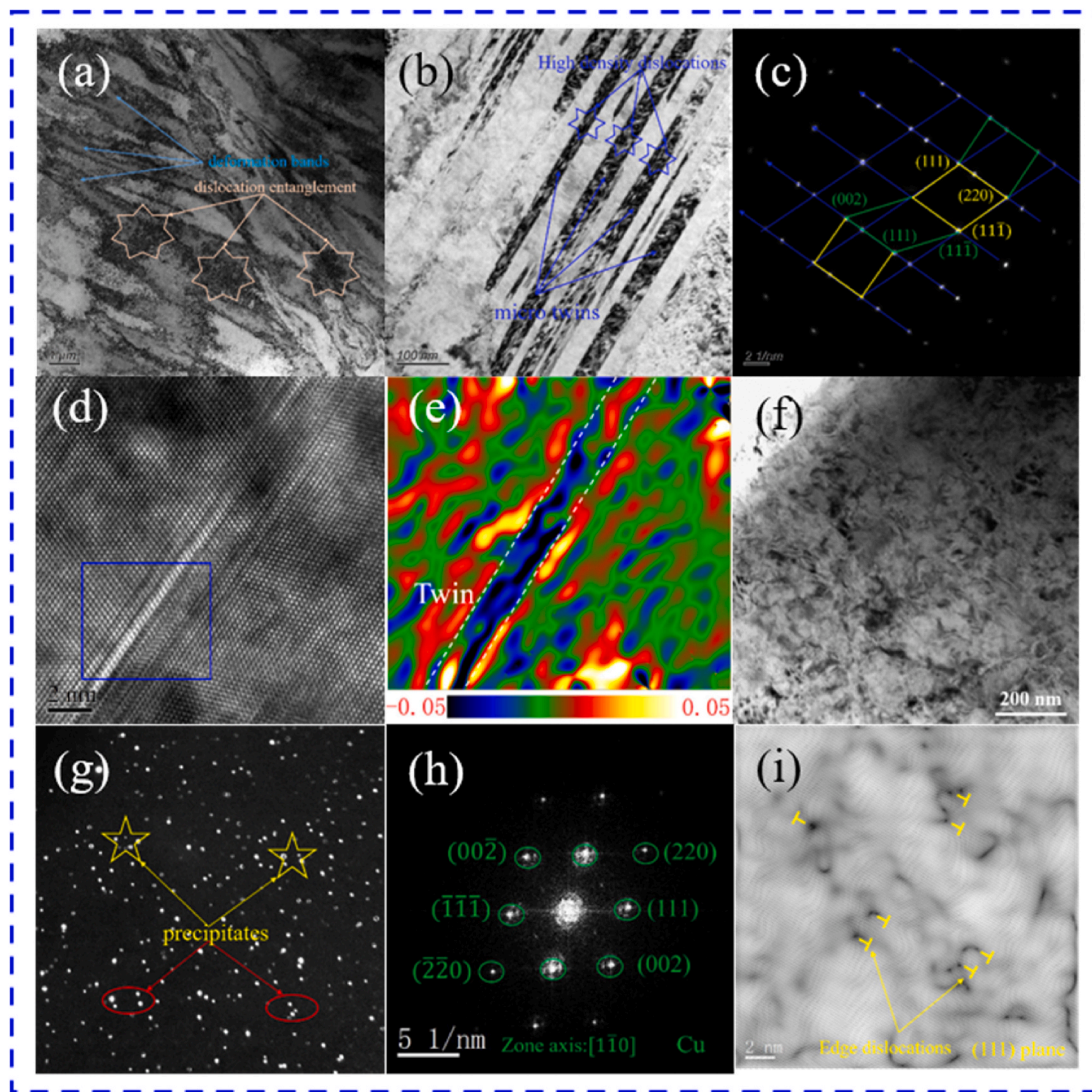

Fig. 10. TEM and HRTEM micrographs of Cu-Co-Si-Ti alloy aging at 500 °C for 30 min: (a) (b) (f) Bright field image, (c) Diffraction spots of twins, (d) HRTEM micrograph of twins, (e) GPA map of blue rectangle in (d), (g) Dark field image showing the precipitates distribution, (h) Diffraction spots of matrix, (g) HRTEM image taken from <111>$_{Cu}$, showing the edge dislocation in the matrix. (For interpretation of the references to colour in this figure legend, the reader is referred to the Web version of this article.)

short-range ordering of Ti atoms occurred in the Cu_4Ti-phase [36]. It can be seen that there was no dislocation from the HRTEM image taken from $<10\bar{1}>_{Cu4Ti}$, as illustrated in Fig. 11(f), which can indicate that the strengthening effect of the second phase particles was non-deformable. When the moving dislocations are met with the second phase particles, they will be blocked by the particles and the dislocation will bend around particles. As the deformation continuing, the bending of dislocations intensified, resulting in the dislocations around the particles meeting at the left and right ends. Ultimately, the positive and negative dislocations offset to form dislocation loops, and the remaining dislocations continued to move forward, as illustrated in Fig. 11(j) for the schematic diagram of dislocations bypassing the second phase particles.

4. Discussion

4.1. Effect of Ti addition on properties and texture

The above results show that the designed Cu-Co-Si-Ti alloy has excellent mechanical and conductivity properties after the cold rolling and aging treatment. In our previous work, it was found that Ti addition can effectively improve the flow stress of Cu-Co-Si alloy during hot deformation, which can be attributed to that the addition of Ti can promote the precipitation, effectively inhibiting the dynamic recovery and recrystallization process [19]. Kim and et al. [29] proved that Ti-alloying improved the mechanical and electrical properties, which was attributed to a decrease of the solution solubility of Ni and Si in the Cu matrix by the formation of smaller and denser δ-Ni_2Si precipitates. During the aging process of Cu-Co-Si and Cu-Co-Si-Ti alloys after cold rolling, the electrical conductivity and micro-hardness with the increasing of aging time, which could be attributed to the effective precipitation due to the high storing energy and enough nucleation sites that formed during the cold rolling process [37]. However, the micro-hardness decreased after exceeding the peak aging time due to the appearance of grown-up precipitates, as illustrated in Fig. 4(a) and (b). Compared Fig. 4(a) with 4(b), it can be observed that the micro-hardness of Cu-Co-Si-Ti alloy in peak aging state was higher than that of Cu-Co-Si alloy due to the Ti addition, increasing from 193 HV (non-Ti doped) to 208 HV (Ti-doped). Moreover, it was more surprising that the addition of Ti accelerated the peak aging rate of the Cu-Co-Si-Ti alloy. The results can be attributed that solute atoms (Co, Si, Ti) continued precipitating from the matrix because of the storing energy and nucleation sites

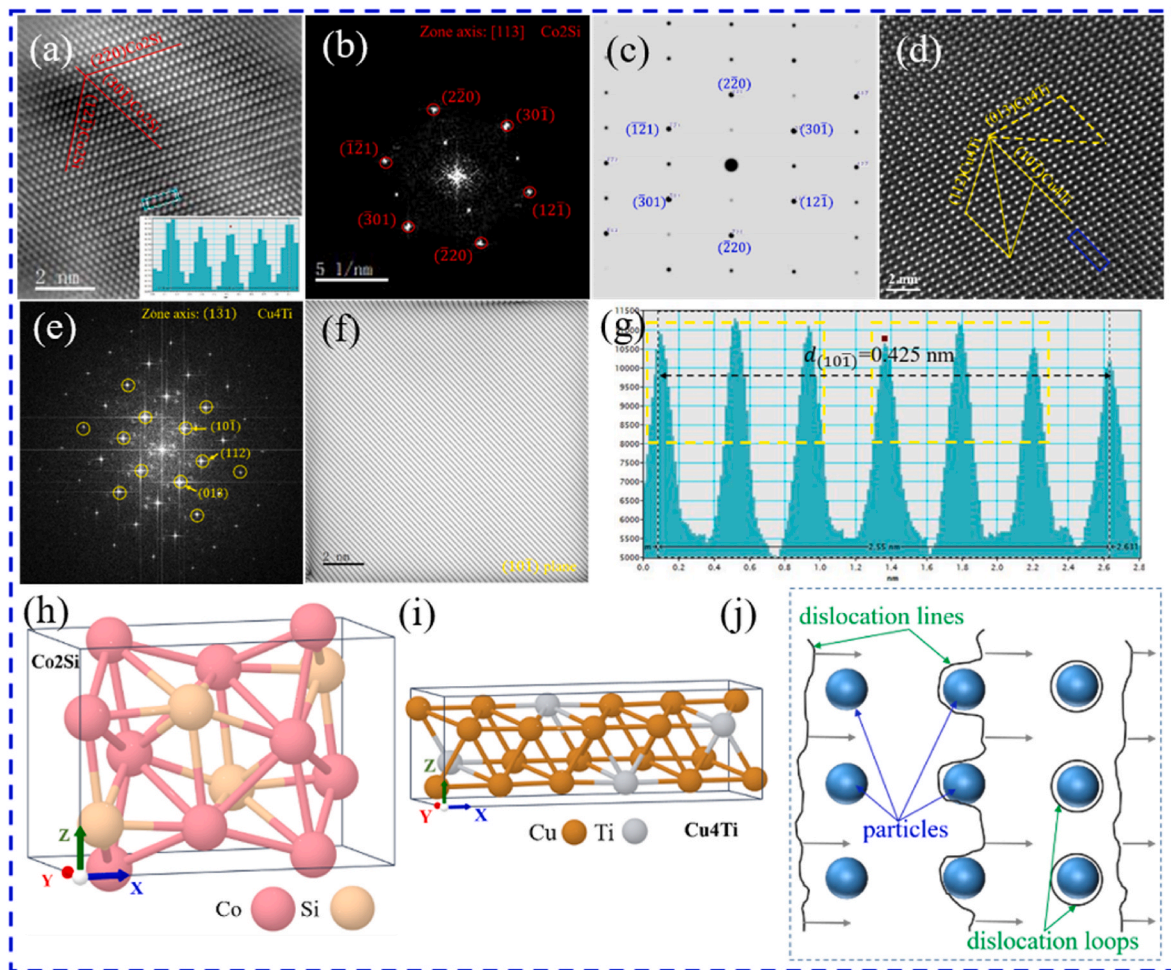

Fig. 11. TEM and HRTEM micrographs of Cu-Co-Si-Ti alloy aging at 500 °C for 30 min: (a) HRTEM image of Co_2Si, (b) (c) FFT pattern of Co_2Si, (d) (f) HRTEM image of Cu_4Ti, (e) FFT pattern of (d), (g) Gray-scale spectrogram of vertical direction of crystal plane in (d), (h) Schematics crystal structure of Co_2Si, (i) Schematics crystal structure of Cu_4Ti, (j) Schematic diagram of dislocations bypassing the second phase particles.

introduced by the cold rolling during the aging process [27]. Moreover, the dynamic interactions among the dislocations and precipitates could definitely improve the mechanical properties of the Cu-Co-Si-Ti alloy [38,39]. Certainly, the addition of Ti can significantly improve the micro-hardness of the Cu-Co-Si-Ti alloy, which was obtained based on sacrificing part of the electrical conductivity of the alloy (Fig. 4(d)).

The addition of Ti not only has a significant effect on the properties of the Cu-Co-Si-Ti alloy, but also effectively influences the microstructure of the Cu-Co-Si-Ti alloy. As given in Fig. 6, it can be observed that there were more twins in the Cu-Co-Si-Ti alloy due to the addition of Ti. The reason may be that the addition of Ti increased the lattice distortion in the Cu matrix and produced higher density dislocations, which made the sliding more difficult and led to more twins (Fig. 6(A3) and (B3)). In addition, due to the Ti addition, the texture underwent substantial changes. It can be observed that the volume fraction for the ideal texture components of Goss texture, Brass texture, copper texture and S texture in Cu-Co-Si alloy were, 4.96%, 14.3%, 15.3% and 9.6%, respectively. Corresponding volume fraction for the ideal texture components of Cu-Co-Si-Ti alloy were 7.01%, 16.4%, 25% and 14.7%, respectively. This caused an increase of the Goss, Brass, copper and S texture components and a substantial decrease of random orientations, indicating a slight texture strengthening. In other words, the main texture components were retained. Similar features have also been observed in copper alloys [40]. In addition, this behavior has also been observed in fcc materials that have been subjected to low and medium rolling degrees [41,42].

4.2. Correlation of texture and mechanical properties

As a result of the rolled sheets subjected to both tensile stress and compressive stress during deformation, some crystallographic directions are parallel to the rolled surface and some crystal planes are parallel to the rolled surface, which have a close relation with the properties of the metallic materials [33,34]. On the one hand, the addition of Ti can significantly improve the micro-hardness of the Cu-Co-Si-Ti alloy, comparing Fig. .4 (a) and (b). On the other hand, Ti addition caused an increase of the Goss, Brass, copper and S texture components and a substantial decrease of random orientations according to Figs. 6 and 7. Moreover, as illustrated in Figs. 8 and 9, the volume fraction of the main texture components for Cu-Co-Si-Ti alloy aging at 30 min, including Goss, Brass, copper and S texture, decreased compared with the aging time of 120 min, whereas the fraction of randomly oriented grains increased, indicating a slight texture weakened. Meanwhile, the above results were accompanied by a characteristic decrease of the micro-hardness (Fig 0.4). Based on the pole figures, 3D ODF maps and changes of main texture components, it can be concluded that the high performance of Cu-Co-Si-Ti alloy can be attributed to the higher volume fraction of Goss, Brass, copper and S texture.

4.3. Strengthening mechanisms

During the heat treatment, the microstructure and the texture underwent substantial changes. In the Cu-Co-Si-Ti alloy, owing to the large

difference of atomic radius between solute atoms (Co, Si, Ti) and copper matrix, lattice distortion occurred in the local crystal of solid solution during solution treatment, resulting in the interaction between stress fields and dislocations and strengthening effect. In the process of cold rolling by 50%, large deformation occurred in the matrix, resulting in the dislocation aggregation, entanglement, formation of dislocation cells and deformation twins, which further strengthen the matrix. Finally, after aging treatment at different time and temperature, the supersaturated solid solution spontaneously decomposed into new phases to further strengthen the matrix, namely multiphase strengthening.

Multiple strengthening mechanisms contributed to the high strength of Cu-Co-Si-Ti alloy. To evaluate the specific contributions of each mechanism, mainly including the solid solution strengthening, work-hardening and precipitation strengthening (Orowan strengthening), the yield strength (σ) of the current Cu-Co-Si-Ti alloy can be given by:

$$\sigma = \sigma_{ss} + \sigma_{ds} + \sigma_p + \sigma_{GB} \tag{1}$$

where σ_{ss} is the stress from solid solution strengthening, σ_{ds} is the stress from work-hardening strengthening, σ_p is the stress from precipitation strengthening, σ_{GB} is the stress from Grain Boundaries.

The melting of solute atoms will cause lattice distortion and different shear modulus, due to the size difference between solute atoms and matrix [43]. The degree of solution strengthening can be described as follows [13]:

$$\sigma_{ss} = G(|\delta| + \frac{1}{20})|\eta|^{\frac{3}{2}}\sqrt{\frac{x_a}{3}} \tag{2}$$

where G is the shear moduli of copper alloy (46 GPa), δ is the factor of lattice change (0.1105), η is the factor describing the change of the shear modulus (0.3171), x_a is the fraction of solute atoms within the solid solution. In this alloy, the fraction of Co, Si and Ti were 1.0%, 0.65% and 0.1%. Hence, the degree of solution strengthening can be calculated as 99.8 MPa.

To further improve the strength of the Cu-Co-Si-Ti alloy, the alloy was subjected to 50% cold rolling after solution treatment, strengthening the copper matrix by dislocation stacking. The degree of work-hardening strengthening can be described as follows [44]:

$$\sigma_{ds} = M\alpha Gb\sqrt{\rho} \tag{3}$$

where M is the Taylor factor (3.06), α is a geometric constant (0.3), G is the shear moduli of copper alloy (46 GPa), b is the Burgers vector of copper alloy (0.2556 nm), ρ is the dislocation density caused by cold deformation, which can be obtained from the KAM map (Fig. (A_3)), calculated by $\rho = 2\theta/_{\mu b}$ $(2 \times 10^{14}\ m^{-2})$. Therefore, the contribution from the work-hardening strengthening can be calculated to be 152 MPa.

The strengthening from the precipitates can be given by the Orowan-Ashby equation [45]:

$$\sigma_p = 0.81 \times \frac{Gb}{2\pi(1-\upsilon)^{1/2}} \times \frac{\ln(d_p/_b)}{(\lambda - d_p)} \tag{4}$$

where G is the shear moduli of copper alloy (46 GPa), b is the Burgers vector of copper alloy (0.2556 nm), ν is the Poisson's ratio (0.34), d_p is the average size of precipitates (9.8 nm), λ is the spacing between particles in the glide plane, which can be expressed by $\lambda = \frac{1}{2}d_p\sqrt{\frac{3\pi}{2f_p}}$. f_p is the volume fraction of the second-phase particles (2.1%). Therefore, the contribution from the precipitation strengthening can be calculated to be 343 MPa.

The movement of dislocations was further hindered by the grains at the boundaries during aging, resulting in a strengthening effect. Grain boundary strengthening can be obtained from the Hall-Petch relationship [46,47]:

$$\sigma_{GB} = K_y d_g^{-1/2} \tag{5}$$

where Ky is the Hall-Petch coefficient (150 MPa μm$^{1/2}$), an expression of the effect of surrounding grains on the flow resistance, and dg is the mean diameter of grain size (25.1 μm in this work). The contribution from the grain boundary strengthening can be calculated to be 30.2 MPa. Ultimately, $\sigma = \sigma_{ss} + \sigma_{ds} + \sigma_p + \sigma_{GB} = 99.8 + 152 + 343 + 30.2 = 625MPa$, there was little difference with the actual measured tensile strength (617.9 MPa).

Microstructure analysis can explain the above reinforcement phenomena for Cu-Co-Si-Ti alloy. With the prolongation of aging time for the same aging temperature (500 °C), on the one hand, the diffusion of atoms promoted the precipitation of new phases to strengthen the matrix (Fig. 5), on the other hand, the micro-hardness decreased slightly due to the effect of dynamic softening (Figs. 3 and 5), whereas the effect of work hardening still existed, which can be seen in Fig. 3 (D) for the texture evolution. Surprisingly, the strengthening degree of precipitation strengthening was larger [17,22], resulting in the high mechanical property during aging due to the multiple strengthening. However, after a certain time (aging for 30 min), the micro-hardness decreased, as a result of the growth of precipitates and increasing dynamic softening effect [7,13,24]. As illustrated in Fig. 3(D), the volume fraction of Goss, Brass, copper and S texture decreased with the aging process. In other words, the texture was further randomized with progressing recrystallization after aging at 500 °C for 2 h. Moreover, the specimen aging for 2 h was hardly capable to store further dislocations, resulting in a strongly decreased work-hardening. In the same aging time, with lower aging temperature, the precipitation power of the second phase was insufficient, and the solute atoms of supersaturated solid solution were difficult to precipitate completely [48], which made the micro-hardness of the Cu-Co-Si-Ti alloy increase slowly (Fig. 2(a)). In the proper aging temperature (500 °C), the de-solvation process of supersaturated solid solution atoms was relatively smooth, which was conducive to the uniform precipitation of the second phase particles. The precipitates were fine and dispersed in the matrix, and the dislocations moved around the particles during deformation, resulting in the significant strengthening effect. When the aging temperature exceeded 500 °C, it will cause the opposite effect, resulting in the decreasing of mechanical properties due to the growth of precipitates and increasing of dynamic softening effect. For the precipitation strengthened copper alloy, the content of solute atoms in the matrix is the main factor affecting the electrical conductivity [2]. The higher content of solute atoms can result in a greater scattering effect on electrons and the lower electrical conductivity. At the initial stage of aging, with the extension of aging time or the increasing of aging temperature, new phases were formed through the diffusion of solute atoms, which made decreasing of the content of solute atoms in the matrix and increasing of the electrical conductivity (as given in Figs. 2(B) and Fig. 5). When all the solute atoms were precipitated, the conductivity still increased with the aging process, which was mainly because the dynamic softening effect of the alloy increased with the holding time for a long time at a certain temperature. The lattice distortion in the matrix decreased and the scattering effect on electrons decreased through the diffusion of atoms, resulting in the continuous increase of electrical conductivity.

5. Conclusions

In summary, high electrical conductivity and excellent mechanical properties of Cu-Co-Si-Ti alloy were obtained by incorporating the multiple alloy elements, resulting in the multiple strengthening during heat treatment. In addition, it can be observed that Ti addition can significantly improve the micro-hardness of Cu-Co-Si-alloy. Based on the achievement of solution strengthening, deformation strengthening and dual-nanoprecipitation strengthening, Cu-Co-Si-Ti alloy acquired the excellent comprehensive performances with the tensile strength of

617.9 MPa and electrical conductivity of 41.7%IACS by cold rolling by 50% and aging at 500 °C for 30 min. Moreover, it was found that the volume fraction of Goss, Brass, copper and S texture had close connections with the mechanical properties by the EBSD technology, which was seldom used in copper alloys during the aging process. By comparing with the contributions of multiple strengthening mechanisms, dual-nanoprecipitation strengthening contributed quite a lot due to the nanoprecipitation of Co_2Si and Cu_4Ti.

CRediT authorship contribution statement

Yongfeng Geng: Experiment, Formal analysis, Writing – review & editing. **Yijie Ban:** Experiment, Formal analysis, Writing – review & editing. **Xu Li:** Formal analysis, Writing – review & editing. **Yi Zhang:** Formal analysis, Writing – review & editing. **Yanlin Jia:** Formal analysis, Writing – review & editing. **Baohong Tian:** Theoretical analysis, Formal analysis, Writing – review & editing. **Meng Zhou:** Theoretical analysis, Formal analysis, Writing – review & editing. **Yong Liu:** Theoretical analysis, Formal analysis, Writing – review & editing. **Alex A. Volinsky:** Theoretical analysis, Formal analysis, Writing – review & editing. **Kexing Song:** Theoretical analysis, Formal analysis, Writing – review & editing.

Declaration of competing interest

The authors declare that they have no known competing financial interests or personal relationships that could have appeared to influence the work reported in this paper.

Acknowledgments

This work was supported by the National Natural Science Foundation of China (52071134), Outstanding Talents Innovation Fund of Henan Province (ZYQR201912164), Key Scientific Research Projects of Higher Education in Henan Province (21A430013) and Natural Science Foundation of Henan Province (202300410144). AV acknowledges support from the Government of the Russian Federation No. 220 of April 09, 2010 (Agreement No. 075-15-2021-612 of June 04, 2021).

References

[1] Y.F. Geng, Y.J. Ban, B.J. Wang, X. Li, K.X. Song, Y. Zhang, Y.L. Jia, B.H. Tian, Y. Liu, A.A. Volinsky, A review of microstructure and texture evolution with nanoscale precipitates for copper alloys, J. Mater. Res. Technol. 9 (5) (2020) 11918–11934.

[2] T. Hu, J.H. Chen, J.Z. Liu, Z.R. Liu, C.L. Wu, The crystallographic and morphological evolution of the strengthening precipitates in Cu-Ni-Si alloys, Acta Mater. 61 (4) (2013) 1210–1219.

[3] Y.J. Ban, Y. Zhang, Y.L. Jia, B.H. Tian, A.A. Volinsky, X.H. Zhang, Q.F. Zhang, Y. F. Geng, Y. Liu, Li Xu, Effects of Cr addition on the constitutive equation and precipitated phases of copper alloy during hot deformation, Mater. Des. 191 (2020), 108613.

[4] Y.Z. Tian, J. Freudenberger, R. Pippan, Z.F. Zhang, Formation of nanostructure and abnormal annealing behavior of a Cu-Ag-Zr alloy processed by high-pressure torsion, Mater. Sci. Eng., A 568 (2013) 184–194.

[5] C.J. Guo, J.S. Chen, X.P. Xiao, H. Huang, W.J. Wang, B. Yang, The effect of Co addition on the modulated structure coarsening and discontinuous precipitation growth kinetics of Cu-15Ni-8Sn alloy, J. Alloys Compd. 835 (2020), 155275.

[6] K.X. Song, Y.F. Geng, Y.J. Ban, Y. Zhang, Z. Li, X.J. Mi, J. Cao, Y.J. Zhou, X. B. Zhang, Effects of strain rates on dynamic deformation behavior of Cu-20Ag alloy, J. Mater. Sci. Technol. 79 (2021) 75–87.

[7] J. Yi, Y.L. Jia, Y.Y. Zhao, Z. Xiao, K.J. He, Q. Wang, M.P. Wang, Z. Li, Precipitation behavior of Cu-3.0Ni-0.72Si alloy, Acta Mater. 166 (2019) 261–270.

[8] Y.C. Cao, S.Z. Han, E.A. Choi, J.H. Ahn, X.J. Mi, S.J. Lee, H. Shin, S.S. Kim, J. Lee, Effect of inclusion on strength and conductivity of Cu-Ni-Si alloys with discontinuous precipitation, J. Alloys Compd. 843 (2020), 156006.

[9] Q. Lei, S.Y. Li, J.L. Zhu, Z. Xiao, F.F. Zhang, Z. Li, Microstructural evolution, phase transition, and physics properties of a high strength Cu-Ni-Si-Al alloy, Mater. Char. 147 (2019) 315–323.

[10] W.N. Liao, X.F. Liu, Y.H. Yang, S.Q. Wang, M. Du, Effect of cold rolling reduction rate on mechanical properties and electrical conductivity of Cu-Ni-Si alloy prepared by temperature controlled mold continuous casting, Mater. Sci. Eng., A 763 (2019), 138608.

[11] Y.K. Wu, Y. Li, J.Y. Lu, S. Tan, F. Jiang, J. Sun, Effects of pre-deformation on precipitation behaviors and properties in Cu-Ni-Si-Cr alloy, Mater. Sci. Eng., A 742 (2019) 501–507.

[12] H. Kim, J.H. Ahn, S.Z. Han, J. Jo, H. Baik, M. Kim, H.N. Han, Microstructural characterization of cold-drawn Cu-Ni-Si alloy having high strength and high conductivity, J. Alloys Compd. 832 (2020), 155059.

[13] Q. Lei, Z. Xiao, W.P. Hu, B. Derby, Z. Li, Phase transformation behaviors and properties of a high strength Cu-Ni-Si alloy, Mater. Sci. Eng., A 697 (2017) 37–47.

[14] W. Wang, H.J. Kang, Z.N. Chen, Z.J. Chen, C.L. Zou, R.G. Li, G.M. Yin, T.M. Wang, Effects of Cr and Zr additions on microstructure and properties of Cu-Ni-Si alloys, Mater. Sci. Eng., A 673 (2016) 378–390.

[15] J. Li, G.J. Huang, X.J. Mi, L.J. Peng, H.F. Xie, Y.L. Kang, Microstructure evolution and properties of a quaternary Cu-Ni-Co-Si alloy with high strength and conductivity, Mater. Sci. Eng., A 766 (2019), 138390.

[16] Z. Zhao, Y. Zhang, B.H. Tian, Y.L. Jia, Y. Liu, K.X. Song, A.A. Volinsky, Co effects on Cu-Ni-Si alloys microstructure and physical properties, J. Alloys Compd. 797 (2019) 1327–1337.

[17] Z.L. Zhao, Z. Xiao, Z. Li, W.T. Qiu, H.Y. Jiang, Q. Lei, Z.R. Liu, Y.B. Jiang, S. J. Zhang, Microstructure and properties of a Cu-Ni-Si-Co-Cr alloy with high strength and high conductivity, Mater. Sci. Eng., A 759 (2019) 396–403.

[18] Y.J. Ban, Y. Zhang, B.H. Tian, K.X. Song, M. Zhou, X.H. Zhang, Y.L. Jia, X. Li, Y. F, Y. Liu, A.A. Volinsky, EBSD analysis of hot deformation behavior of Cu-Ni-Co-Si-Cr alloy, Mater. Char. 169 (2020), 110656.

[19] Y.F. Geng, X. Li, H.L. Zhou, Y. Zhang, Y.L. Jia, B.H. Tian, Y. Liu, A.A. Volinsky, X. H. Zhang, K.X. Song, G.X. Wang, L.H. Li, J.R. Hou, Effect of Ti addition on microstructure evolution and precipitation in Cu-Co-Si alloy during hot deformation, J. Alloys Compd. 821 (2020), 153518.

[20] Y.F. Geng, Y. Zhang, K.X. Song, Y.L. Jia, X. Li, H.R. Stock, H.L. Zhou, B.H. Tian, Y. Liu, A.A. Volinsky, X.H. Zhang, P. Liu, X.H. Chen, Effect of Ce addition on microstructure evolution and precipitation in Cu-Co-Si-Ti alloy during hot deformation, J. Alloys Compd. 842 (2020), 155666.

[21] Satoshi Semboshi, Shigeo Sato, Akihiro Iwase, Takayuki Takasugi, Discontinuous precipitates in age-hardening CuNiSi alloys, Mater. Char. 115 (2016) 39–45.

[22] J. Chalon, J.D. Guérin, Dubar, L. Dubois, A. Puchi-Cabrera, Characterization of the hot-working behavior of a Cu-Ni-Si alloy, Mater. Sci. Eng., A 667 (2016) 77–86.

[23] D.P. Lu, J. Wang, W.J. Zeng, Y. Liu, L. Lu, B.D. Sun, Study on high-strength and high-conductivity Cu-Fe-P alloys, Mater. Sci. Eng., A 421 (2006) 254–259.

[24] B.J. Wang, Y. Zhang, B.H. Tian, Y.L. Jia, Alex A. Volinsky, V. Yakubovd, Y. Liu, K. X. Song, M. Fu, Nanoscale precipitates evolution and strengthening mechanism of the aged Cu-Mg-Fe-Sn-P-Y electrical contact wire, J. Mater. Res. Technol. 9 (3) (2020) 6352–6359.

[25] J.C. An, B.J. Wang, Y. Zhang, B.H. Tian, Alex A. Volinsky, Y. Liu, G.X. Wang, Mechanical and electrical properties and phase Analysis of aged Cu-Mg-Ce alloy, J. Mater. Eng. Perform. 29 (2020) 1–9.

[26] J.Y. Cheng, B.B. Tang, F.X. Yu, B. Shen, Evaluation of nanoscale precipitates in a Cu-Ni-Si-Cr alloy during aging, J. Alloys Compd. 614 (2014) 189–195.

[27] J.Z. Huang, Z. Xiao, J. Dai, Z. Li, H.Y. Jiang, W. Wang, X.X. Zhang, Microstructure and properties of a novel Cu-Ni-Co-Si-Mg alloy with super-high strength and conductivity, Mater. Sci. Eng., A 744 (2019) 754–763.

[28] J. Liu, X.H. Wang, J. Chen, J.T. Liu, The effect of cold rolling on age hardening of Cu-3Ti-3Ni-0.5Si alloy, J. Alloys Compd. 797 (2019) 370–379.

[29] H.G. Kim, T.W. Lee, S.M. Kim, S.Z. Han, K. Euh, W.Y. Kim, S.H. Lim, Effects of Ti addition and heat treatments on mechanical and electrical properties of Cu-Ni-Si alloys, Met. Mater. Int. 19 (2013) 61–65.

[30] E. Lee, K. Euh, S.Z. Han, S. Lim, J. Lee, S. Kim, Tensile and electrical properties of direct aged Cu-Ni-Si-x%Ti alloys, Met. Mater. Int. 19 (2013) 183–188.

[31] Y.K. Xie, Y.L. Deng, Y. Wang, X.B. Guo, Effect of asymmetric rolling and subsequent ageing on the microstructure, texture and mechanical properties of the Al-Cu-Li alloy, J. Alloys Compd. 836 (2020), 155445.

[32] S.L. Fu, P. Liu, X.H. Chen, H.L. Zhou, F.C. Ma, W. Li, K. Zhang, Effect of aging process on the microstructure and properties of Cu-Cr-Ti alloy, Mater. Sci. Eng., A 802 (2021), 140598.

[33] C. Haase, L.A. Barrales-Mora, Influence of deformation and annealing twinning on the microstructure and texture evolution of face-centered cubic highentropy alloys, Acta Mater. 150 (2018) 88–103.

[34] J. Liu, X.h. Wang, J. Chen, J.T. Liu, The effect of cold rolling on age hardening of Cu-3Ti-3Ni-0.5Si alloy, J. Alloys Compd. 797 (2019) 370–379.

[35] Y. Fu, W.L. Xiao, D. Kent, M.S. Dargusch, J.S. Wang, X.Q. Zhao, C.L. Ma, Ultrahigh strain hardening in a transformation-induced plasticity and twinning-induced plasticity titanium alloy, Scripta Mater. 187 (2020) 285–290.

[36] Y.W. Song, M.J. Jin, X.C. Han, X.D. Wang, P. Chen, X.J. Jin, Microstructural origin of ultrahigh damping capacity in Ni50.8Ti49.2 alloy containing nanodomains induced by insufficient annealing and low-temperature aging, Acta Mater. 205 (2021), 116541.

[37] Q. Lei, Z. Li, Y. Gao, X. Peng, B. Derby, Microstructure and mechanical properties of a high strength Cu-Ni-Si alloy treated by combined aging processes, J. Alloys Compd. 695 (2017) 2413–2423.

[38] S. Nagarjuna, K. Balasubramanian, D.S. Sarma, Effect of prior cold work on mechanical properties, electrical conductivity and microstructure of aged Cu-Ti alloys, J. Mater. Sci. 34 (12) (1999) 2929–2942.

[39] H.Y. Yang, K.Q. Li, Y.Q. Bu, J.M. Wu, Y.T. Fang, L. Meng, J.B. Liu, H.T. Wang, Nanoprecipitates induced dislocation pinning and multiplication strategy for designing high strength, plasticity and conductivity Cu alloys, Scripta Mater. 195 (2021), 113741.

[40] J.F. Savoie, Einfluss des Zinkgehaltes und der Korngrosse auf die Walz-und Rekristallisationstexturentwicklung in a-Messing, Institute of Physical Metallurgy and Metal Physics, RWTH Aachen University, 1990.
[41] C. Haase, L.A. Barrales-Mora, D.A. Molodov, G. Gottstein, Application of texture analysis for optimizing thermo-mechanical treatment of a high Mn TWIP Steel, Adv. Mater. Res. 922 (2014) 213.
[42] M. Klimova, S. Zherebtsov, N. Stepanov, G. Salishchev, C. Haase, D.A. Molodov, Microstructure and texture evolution of a high manganese TWIP steel during cryo-rolling, Mater. Char. 132 (2017) 20.
[43] Z. Wu, Y. Gao, H. Bei, Thermal activation mechanisms and Labusch-type strengthening analysis for a family of high-entropy and equiatomic solid-solution alloys, Acta Mater. 120 (2016) 108–119.
[44] Z.W. Wang, W.J. Lu, H. Zhao, C.H. Liebscher, J.Y. He, D. Ponge, D. Raabe, Z.M. Li, Ultrastrong lightweight compositionally complex steels via dual-nanoprecipitation, Sci. Adv. 6 (2020) 1–7.
[45] M. Mabuchi, K. Higashi, Strengthening mechanism of Mg-Si alloy, Acta Mater. 44 (1996) 4611–4618.
[46] Y. Zhang, N.R. Tao, K. Lu, Mechanical properties and rolling behaviors of nanograined copper with embedded nano-twin bundles, Acta Mater. 56 (2008) 2429–2440.
[47] N. Hansen, Hall-Petch relation and boundary strengthening, Scripta Mater. 51 (2004) 801–806.
[48] J.C. Zhao, M.R. Notis, Spinodal decomposition, ordering transformation, and discontinuous precipitation in a Cu-15Ni-8Sn alloy, Acta Mater. 46 (12) (1998) 4203–4218.